
Synthetic Data as Validation

Qixin Hu

The Chinese University of Hong Kong
qixinhu@cuhk.edu.hk

Alan Yuille

Johns Hopkins University
ayuille1@jhu.edu

Zongwei Zhou*

Johns Hopkins University
zzhou82@jh.edu

Abstract

This study leverages synthetic data as a validation set to reduce overfitting and ease the selection of the best model in AI development. While synthetic data have been used for augmenting the training set, we find that synthetic data can also significantly diversify the validation set, offering marked advantages in domains like healthcare, where data are typically limited, sensitive, and from out-domain sources (i.e., hospitals). In this study, we illustrate the effectiveness of synthetic data for early cancer detection in computed tomography (CT) volumes, where synthetic tumors are generated and superimposed onto healthy organs, thereby creating an extensive dataset for rigorous validation. Using synthetic data as validation can improve AI robustness in both in-domain and out-domain test sets. Furthermore, we establish a new continual learning framework that continuously trains AI models on a stream of out-domain data with synthetic tumors. The AI model trained and validated in dynamically expanding synthetic data can consistently outperform models trained and validated exclusively on real-world data. Specifically, the DSC score for liver tumor segmentation improves from 26.7% (95% CI: 22.6%–30.9%) to 34.5% (30.8%–38.2%) when evaluated on an in-domain dataset and from 31.1% (26.0%–36.2%) to 35.4% (32.1%–38.7%) on an out-domain dataset. Importantly, the performance gain is particularly significant in identifying very tiny liver tumors (radius < 5mm) in CT volumes, with Sensitivity improving from 33.1% to 55.4% on an in-domain dataset and 33.9% to 52.3% on an out-domain dataset, justifying the efficacy in early detection of cancer. The application of synthetic data, from both training and validation perspectives, underlines a promising avenue to enhance AI robustness when dealing with data from varying domains. As open science, we have released the codes and models at <https://github.com/MrGiovanni/SyntheticValidation>.

*Corresponding author

1 Introduction

Standard AI development divides the dataset into a training set and a test set; the former is used for model training and the latter for evaluation (Russell, 2010; Gareth et al., 2013). The AI model is updated every *training epochs*, resulting in a number of intermediate models during the training trajectory. The performance of these models tends to improve on the training set, but this does not mean that the performance on the test set also improves due to the over-fitting problem (Kuhn et al., 2013). A question then arises: *How do we identify the best model that performs well on the test set, especially when it is evaluated on test sets taken from different domains?* A prevalent strategy is to delineate a validation set from the training set (Ripley, 2007). This validation set neither contributes to training nor to evaluating the AI performance. Instead, it functions as an independent set to fix the training hyper-parameters and, more importantly, to estimate the performance of each model on different datasets, thus enabling the selection of the best model from the many intermediate models during the training trajectory.

The validation set is often kept small. Naturally, we would like to maximize the use of the training data. Annotating data for AI training is time-consuming and expensive, requiring specialized expertise, so the annotated datasets are limited in size in many fields (Zhou, 2021). Allocating too many annotated data for validation would inevitably diminish the training set size and compromise the AI training. On the other hand, the validation set should be sufficiently representative to provide a reliable performance estimate on unseen data. An overly small validation set might risk the reliability of performance estimation and checkpoint selection. As a result, the calibration of the validation set remains largely empirical and lacks systematic investigation for better alternatives to select the best checkpoint. Fulfilling this knowledge gap is particularly important in scenarios where real-world data are scarce, sensitive, or costly to collect and annotate, as seen in the field of *AI for healthcare* (Zhou et al., 2022). Therefore, our study uses early detection of cancerous tumors in computed tomography (CT) volumes as a demonstration. While early detection of cancer holds immense clinical potential, it faces profound constraints like disease prevalence and annotation difficulty to collect examples of early-stage tumors (Crosby et al., 2022). The scarcity of annotated early cancer not only constrains the data available for validation but also amplifies the overfitting problem inherent in a small, biased validation set, potentially causing underdiagnosis and overdiagnosis.

We propose using synthetic data as validation, a strategy that guarantees the full utilization of the training set while ensuring ample data diversity for validation. Data synthesis has held longstanding interest and presents numerous intriguing merits for augmenting training and test data (Hu et al., 2023; Gao et al., 2023) as reviewed in §2, but its use in validation has seldom been explored. We find that synthetic data can facilitate a more reliable performance estimate on unseen data and effectively address the constraints commonly associated with small, biased validation sets. Specifically, we synthesize tumors in the healthy liver, which gives us orders of magnitude larger datasets for training. To ensure the realism of the synthetic tumors, we employ a modeling-based strategy (Hu et al., 2023) to simulate cancerous tumors with controlled shape, size, texture, location, and intensity. The use of diverse, healthy CT volumes, supplemented with synthetic tumors, as validation has demonstrated efficacy in mitigating model overfitting and enhancing the selection of checkpoints. Furthermore, we relieve the pressing demand for human annotations to train AI models by utilizing CT volumes with synthetic tumors as the training set. We then assess the model’s performance using a substantial number of publicly available, fully-annotated CT volumes with real-world cancerous tumors, showing that our models generalize well to these volumes from different hospitals and accurately segment the tumors at their early stage. Our findings can be summarized as follows:

1. The best model checkpoint, selected by standard AI development with an in-domain real-tumor validation set, may not necessarily be generalized to unseen data, especially for an out-domain test set. This limitation arises from the validation set failing to adequately represent corner cases.
2. The best model checkpoint, selected by our strategy with a diverse synthetic-tumor validation set, tends to be generalized well to unseen data. This is because the validation set can cover theoretically infinite examples of possible cancerous tumors across diverse conditions.
3. We introduce a novel continual learning framework. This framework integrates a continuous stream of synthetic data, characterized by diverse data distribution, for both training and validation. Traditional validation sets, constrained by static and limited in-domain real tumors, fall short in such a setting, whereas our synthetic tumors can be dynamically tailored to align with emerging distributions. Importantly, our framework can continuously generate tumors spanning a spectrum of sizes—from small to large—enhancing the detection rate of tumors at their early stages.

Although our study focuses on AI in healthcare, the insight should be pertinent to various imaging applications within the field of computer vision. However, at the time this paper is written, very few studies in computer vision have provided evidence that training *exclusively* on generated synthetic data can match or surpass the performance achieved when trained on real data (Black et al., 2023). In specific applications, integrating synthetic data with real

data—essentially acting as data augmentation—has been found empirically to boost AI performance (Mu et al., 2020; Luzzi et al., 2022; Azizi et al., 2023; Burg et al., 2023). In this regard, data synthesis—cancerous tumor synthesis in particular—in medical imaging is relatively more successful¹ with specific applications benefiting more from training exclusively on synthetic data than real data.

2 Related Work

The dilemma of validation.

In the field of machine learning, it is customary to use finite, static datasets with a pre-defined data split. While this standard offers a fair benchmark for comparing different AI models, it does not accurately represent real-world learning conditions. Two more realistic scenarios often arise in practice.

- The first scenario is the *small data regime*, commonly observed in medical applications due to constraints like disease prevalence and annotation difficulty (Liu et al., 2022). In such cases, curating an appropriate validation set poses a conundrum. A large validation set would compromise the size of the training set, whereas a small one may not sufficiently estimate the model’s performance. Despite its critical importance, this issue has yet to receive adequate attention in the field.
- The second scenario involves dealing with *a stream of data*, in a context of continual learning where the model encounters a continuous flow of new data (Purushwalkam et al., 2022). A finite, static validation set proves unsuitable as it cannot accurately assess the model’s capability in processing an extensive and diverse data range. We argue that a validation set—made up of real-world data—might not be needed during the training stage in such situations. Given the vastness of the training data, overfitting can be naturally avoided. Consequently, selecting the last-epoch model checkpoint could be a judicious choice.

Progresses in data synthesis. Real-world data often encounters challenges such as poor quality, limited quantity, and inaccessibility (Zhu et al., 2022; Qu et al., 2023; Kang et al., 2023; Liu et al., 2023a). To tackle these obstacles, the notion of *synthetic data* has emerged as a practical alternative, allowing for the generation of samples as needed (Jordon et al., 2018; Yoon et al., 2019; Chen et al., 2021). This approach has proven valuable in addressing data limitations and facilitating machine learning processes, including computer vision (Chen et al., 2019; Ramesh et al., 2021), natural language processing (Collobert and Weston, 2008; Brown et al., 2020), voice (Oord et al., 2016), and many other fields (Wiese et al., 2020; Jin et al., 2018; Zheng et al., 2023). In the medical domain, the practice of data synthesis—*tumor synthesis* in particular—endeavors to produce artificial tumors in the image, which can significantly diversify the data and annotations for AI training (Xing et al., 2023) and, arguably, can strengthen the AI robustness evaluation using corner cases generated by data synthesis. Successful works related to tumor synthesis include polyp detection from colonoscopy videos (Shin et al., 2018), COVID-19 detection from Chest CT and X-ray (Yao et al., 2021; Lyu et al., 2022; Gao et al., 2023), diabetic lesion detection from retinal images (Wang et al., 2022), cancer detection from fluorescence microscopy images (Horvath et al., 2022), brain tumor detection from MRI (Wyatt et al., 2022), early pancreatic cancer localization from CT (Li et al., 2023), and pneumonia detection from ultrasound (Yu et al., 2023). A recent study (Hu et al., 2022, 2023) indicated that AI trained *exclusively* on synthetic tumors can segment liver tumors with accuracy comparable to that on real tumors.

To the best of our knowledge, data synthesis has been widely recognized for its contribution to enhancing training and test datasets (Johnson et al., 2017; Jordon et al., 2022; Liu et al., 2023b), but its capacity for improving the validation set remains largely untapped. In this paper, we extend the application of synthetic data to the validation set, enabling the full use of the annotated data for AI training while ensuring diverse and comprehensive validation data in the framework of continual learning.

3 Method & Material

3.1 Continual Learning for Tumor Segmentation

According to Van de Ven and Tolias (2019); Van de Ven et al. (2022), continual learning can be categorized into three settings: class-incremental learning, task-incremental learning, and domain-incremental learning. In the domain-incremental setting, which is relevant to our situation, the task remains the same while the data distribution changes. More specifically, the model sequentially encounters data from a continuum of domains (datasets):

$$\{X_1, Y_1\}, \{X_2, Y_2\}, \dots, \{X_N, Y_N\}, \quad (1)$$

¹The greater success of data synthesis in medical imaging (reviewed in §2), compared with computer vision, can be attributed to two factors from our perspective. Firstly, the focus is primarily on synthesizing tumors rather than other components of the human anatomy. Secondly, the synthesis of tumors in 3D medical images is less complex as it does not require considerations for intricate variables such as lighting conditions, pose, and occlusion, which are typical in computer vision tasks.

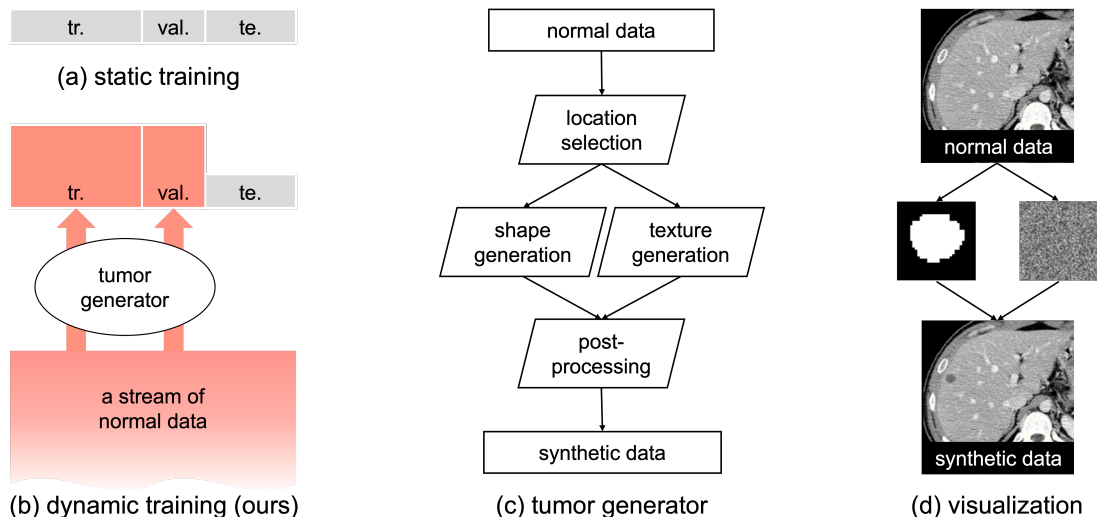


Figure 1: **Illustration of continual learning framework.** (a) The setting for the static training, where the real-tumor dataset is partitioned into training and validation sets. The AI model is then developed using these datasets and subsequently tested with unseen data. (b) Dynamic training setting integrated with synthetic data. (c) Tumor generator pipeline. By leveraging an advanced tumor generator, we can create a dynamic training and validation set. Models developed using the continual learning framework exhibit superior performance compared to static training settings. (d) Visualization of synthetic data.

The objective is to train a model $\mathcal{F} : X \rightarrow Y$ that can be effectively queried at any given time, regardless of the data distribution. In liver tumor segmentation tasks, X is the CT volume and Y is the tumor mask. The continuum of domains refers to CT volumes taken from different medical centers.

In the setting of *static* training, shown in Figure 1(a), the AI model is trained and validated on fixed subsets of a dataset. This setting presents three limitations: Firstly, the limited scales and acquisition sources of the data, coupled with unchanged data distribution, pose challenges in generalizing to out-domain data. Secondly, the task of data annotation, specifically tumor annotation, is exceptionally challenging as it often requires the use of corroborative pathology reports. This requirement adds to the difficulty of extending the dataset. Thirdly, there are specific cases, such as extremely small tumors, where obtaining real data becomes significantly challenging. As a result, static training will likely result in biased, sub-optimal performance on unseen data, especially for out-domain test sets.

In contrast, the setting of *dynamic* training achieved by synthetic data, shown in Figure 1(b), can overcome the aforementioned limitations. In this setting, the AI model is trained and validated on a dynamically changing dataset. In our study, this dynamic dataset is a stream of normal CT volumes—over 40 million CT volumes in the United States each year. Generating synthetic tumors is advantageous because, firstly, acquiring healthy CT volumes is much easier than obtaining those with cancerous tumors. As a result, our continual learning framework can start from a diverse dataset comprising CT volumes of healthy subjects from multiple domains. Secondly, by controlling the parameters within our framework, we have the ability to generate synthetic data that fulfills specific requirements, including those of a tiny radius (<5 mm, shown in Appendix Figure 9). Consequently, our framework achieves a noteworthy level of diversity, encompassing a wide array of variations. Therefore, the AI model developed using this framework of synthetic data has the potential to improve its performance on out-domain data.

3.2 Modeling-Based Synthetic Tumor Generation

Following the standardized clinical guidance and statistical distribution of real tumors, as detailed in Appendix Figure 7 8, we develop a modeling-based strategy to generate synthetic tumors. For example, according to the Liver Imaging Reporting and Data System (LI-RADS) (Chernyak et al., 2018), the malignancy of hepatocellular carcinomas is determined by shape, size, location, and texture, enhancing capsule appearance. We use a sequence of morphological image-processing operations to model real tumors, as shown in Figure 1(c). The tumor generator consists of four steps: (1) location selection, (2) shape generation, (3) texture generation, and (4) post-processing.

1. **Location selection.** Liver tumors generally do not allow the passage of preexisting blood vessels from the host tissue through them. To address this concern, we initially perform voxel value thresholding for vessel segmentation (Gonzalez, 2009). Utilizing the vessel mask acquired from this step enables us to identify if a particular location can cause the tumor-blood collision.
2. **Shape generation.** Based on clinical knowledge, a tumor is initiated from a malignant cell and gradually

proliferates and expands, resulting in a nearly spherical shape for small tumors ($\leq 5\text{mm}$). On the other hand, statistical distributions of real liver tumors indicate that larger tumors tend to exhibit an elliptical shape. This observation has inspired us to generate a tumor-like shape using an ellipsoid $ellip(a, b, c)$, where a, b, c are the lengths of the semi-axes. Additionally, we utilize elastic deformation (Ronneberger et al., 2015) to enhance the authenticity of the generated tumor shapes $D(ellip(a, b, c), \sigma_d)$, where σ_d control the magnitude of displacements. We show examples of the generated tumor shapes in Appendix Figure 9.

3. **Texture generation.** The generation of textures is a significant challenge due to the varied patterns found in tumors. Our current understanding of tumor textures is derived solely from clinical expertise, which considers factors such as the attenuation value and the distribution characteristics. To achieve the desired texture, we introduce Gaussian noise $\mathcal{N}(\mu, \sigma_g)$ with a predetermined mean attenuation value, matching the standard deviation of liver tumors. Subsequently, we use cubic interpolation to smooth the texture. Furthermore, to better replicate textures obtained from CT imaging, we use a final step of texture blurring. Examples of the generated texture can be found in Appendix Figure 10.
4. **Post-processing.** The post-processing involves evaluating image characteristics through visual inspection and feedback from medical professionals. The purpose of these steps is to replicate the phenomena of mass effect and the appearance of a capsule (Lee et al., 2004). Mass effect refers to the phenomenon wherein the tumor undergoes growth, resulting in the displacement and deformation of surrounding tissues. We utilize local scaling warping (Glasbey and Mardia, 1998) to replicate this effect. Additionally, we brighten the edges of the tumor, thereby simulating the capsule appearance. Consequently, CT volumes with synthetic tumors can be used for the continual learning framework, where examples of the generated liver tumors can be found in Appendix Figure 11.

4 Experiment

4.1 Dataset & Benchmark

Table 1: **Datasets description.** The LiTS dataset was used to train, validate, and evaluate AI models in segmenting liver tumors. The FLARE’23 dataset was used for external validation. An assembly of the CHAOS (Valindria et al., 2018), BTCV (Landman et al., 2015), and Pancreas-CT (Roth et al., 2016) datasets were used for generating synthetic training and validation sets, in which the liver in these datasets is confirmed to be healthy.

dataset	notation	split	annotation	# of CTs	tumor
LiTS (Bilic et al., 2019)	cohort 1	training	✓	25	real
	cohort 2	validation	✓	5	real
	cohort 3	testing	✓	70	real
Assembly (Hu et al., 2023)	cohort 4	training	✗	25	synthetic
	cohort 5	validation	✗	50	synthetic
FLARE’23 (Ma et al., 2022)	cohort 6	validation	✗	50	synthetic
	cohort 7	testing	✓	120	real

Table 1 summarizes a total of five publicly available datasets used in this study. We group them into three classes.

- **Real-tumor dataset.** We select the LiTS dataset (Bilic et al., 2019) for training and testing AI models. LiTS provides detailed per-voxel annotations of liver tumors. The tumor types include HCC and secondary liver tumors and metastasis derived from colorectal, breast, and lung cancer. The size of liver tumors ranges from 38mm^3 to 349cm^3 , and the radius of tumors is approximately in the range of $[2, 44]$ mm. LiTS is partitioned into a training set (*cohort 1*; 25 CT volumes), validation set (*cohort 2*; 5 CT volumes), and test set (*cohort 3*; 70 CT volumes).
- **Healthy CT assembly.** We have collected a dataset of 75 CT volumes with healthy liver assembled from CHAOS (Valindria et al., 2018), Pancreas-CT (Roth et al., 2016) and BTCV (Landman et al., 2015). This assembled dataset is partitioned into a training set (*cohort 4*; 25 CT volumes) and a validation set (*cohort 5*; 50 CT volumes). As illustrated in Figure 1(b) For the training set, tumors were dynamically generated within these volumes during training, resulting in a sequential collection of image-label pairs comprising synthetic tumors. For the validation set, we generated three different tumor sizes (small, medium, and large) for each healthy CT volume offline, giving a total of 150 CT volumes.
- **External benchmark.** FLARE’23 (Ma et al., 2022) is used for an external benchmark because it provides out-domain CT volumes from the LiTS dataset. This dataset was specifically chosen due to its extensive coverage, encompassing over 4000 3D CT volumes obtained from more than 30 medical centers. The inclusion of such a

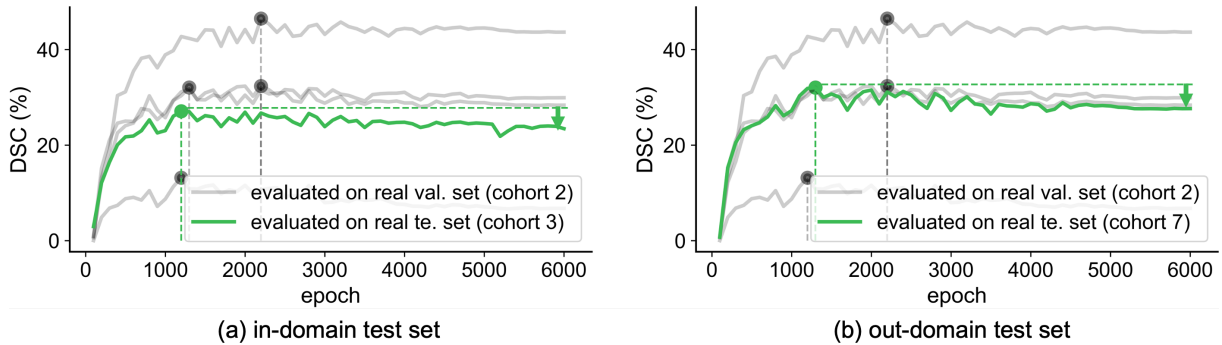


Figure 2: **The overfitting is due to a small-scale, biased real-tumor validation set.** Model checkpoints are saved at each training epoch, and their performance trajectories are evaluated. The **green** curve plots the test set performance of each checkpoint. It serves as the gold standard for a specific dataset, though the test set performance is often apriori unknown. The **gray** curve plots the validation set performance of each checkpoint. This performance is accessible during the AI training and instrumental in selecting the best model checkpoint. We train a model on the LiTS training set and subsequently test it on the LiTS test set as in-domain evaluation **(a)** and the FLARE’23 dataset as out-domain evaluation **(b)**. At the initial epochs, the model performs increasingly well, but its test set performance declines when trained for more epochs, highlighted by the green arrow. This decline is attributed to *overfitting*, where the model becomes too specialized on the training set and loses its ability to generalize effectively to the test set. The purpose of a validation set is to select the best model checkpoint that is expected to perform well on unseen data. However, in practice, the size and diversity of the validation set may be limited, leading to potential inaccuracies in checkpoint selection. This is evidenced by both in-domain **(a)** and out-domain **(b)** evaluations. The dots on the curve represent the best checkpoint selected by the test set (**green**) or the real-tumor validation (**gray**). A comparative analysis reveals that the checkpoints selected based on the real-tumor validation set might not be the most suitable for test sets.

diverse dataset ensures the generalizability of the benchmark. The FLARE’23 dataset contains partially labeled annotations. To ensure the suitability of the test set, specific criteria are applied to the annotations. These criteria require that the annotations include per-voxel labeling for both the liver and tumors, with the additional constraint that the connected component of the tumor must intersect with the liver. Adhering to these conditions, we chose the external test set (*cohort 7*; 120 CT volumes). Additionally, same as the assembly dataset, we can use the healthy cases within the FLARE’23 to generate synthetic data to serve as *in-domain* validation set (*cohort 6*; 50 CT volumes), which will be used in §5.5.

4.2 Implementation

We have implemented our codes utilizing the MONAI² framework for the U-Net architecture (Ronneberger et al., 2015), a well-established network commonly employed in medical image segmentation tasks. During the pre-processing stage, input images undergo clipping with a window range of $[-21, 189]$. Following this, they are normalized to achieve a zero mean and unit standard deviation (Tang et al., 2022). For training purposes, random patches with dimensions of $96 \times 96 \times 96$ are cropped from the 3D image volumes. A base learning rate of 0.0002 is utilized in the training process, accompanied by a batch size of two per GPU. To further enhance the training process, we employ both the linear warmup strategy and the cosine annealing learning rate schedule. Our model is trained for 6,000 epochs, with a model checkpoint being saved every 100 epochs, and a total of 60 model checkpoints are saved throughout the entire training process. During the inference phase, a sliding window strategy with an overlapping area ratio of 0.75 is adopted. To ensure robustness and comprehensiveness in obtaining results, the experiment is conducted ten times each to perform statistical analysis. By averaging all runs, we obtain reliable results. The segmentation performance is evaluated using the Dice Similarity Coefficient (DSC) score, while Sensitivity is used to evaluate the performance of detecting very tiny liver tumors (radius $< 5\text{mm}$).

5 Result

Summary. Using synthetic data as validation can select the best model checkpoint and alleviate the overfitting problem. Furthermore, the AI model developed using our continual learning framework outperforms models trained and validated on a static dataset. The performance is particularly high for detecting small/tiny tumors because we can generate a vast number of examples of small/tiny tumors for both training and validation.

²<https://monai.io/>

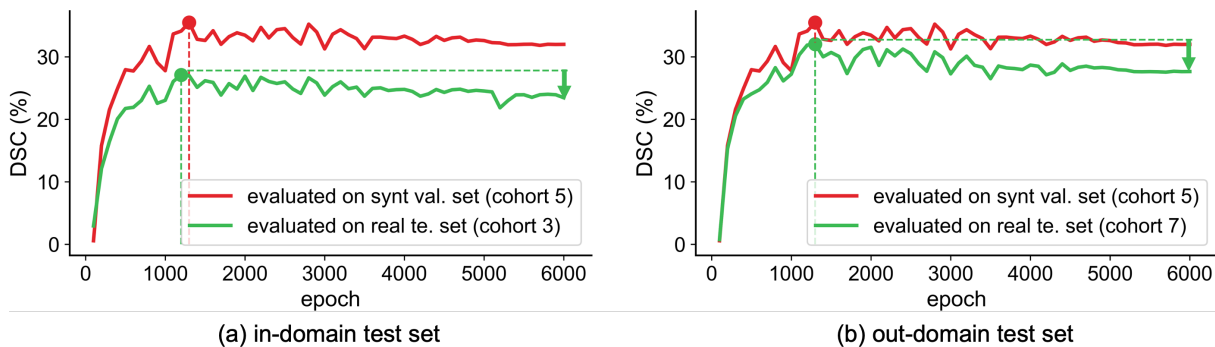


Figure 3: **The overfitting is alleviated by a large-scale, synthetic-tumor validation set.** Similar to Figure 2, (a) and (b) denote in-domain and out-domain evaluations, and the green curves are the test set performance on these two datasets—serving as the gold standard for checkpoint selection. The red curves are the validation performance using synthetic tumors (cohort 5). In theory, we can generate an unlimited number of tumors in varied conditions, e.g., size, location, shape, and texture, as needed, using the tumor generator described in §3.2. Such extensive coverage enhances the ability of the validation set to estimate how well the model can be generalized to previously unseen data distributions. As shown in both in-domain and out-domain evaluation, synthetic data as validation can accurately select the best model checkpoint that is almost identical to that selected by test sets.

5.1 Overfitting is Attributed to Small-Scale, Real-Tumor Validation

To demonstrate the potential limitations of selecting the best model checkpoint based on a small-scale and biased real-tumor validation set, we evaluate all the model checkpoints in real-tumor validation set (cohort 2), in-domain LiTS test set (cohort 3) and out-domain FLARE’23 test set (cohort 7). In-domain test set (cohort 3) assesses the performance of each checkpoint and aids in determining the effectiveness of the selected best checkpoints using the validation set (cohort 2). Out-domain test set (cohort 7) serves as a robust benchmark, providing an enhanced evaluation of the performance of the model checkpoints on out-domain unseen data.

As shown in Figure 2, two significant observations can be made. Firstly, the best checkpoint identified by the small-scale real-tumor validation set exhibits considerable instability, with notable variations observed when different validation samples are chosen. This result indicates that the small-scale real-tumor validation is inherently biased and lacks the ability to adequately represent the broader range of cases. Secondly, the performance of the best checkpoint determined by the real validation set does not effectively generalize to unseen test data, particularly when confronted with out-domain data. These observations indicate that overfitting can be attributed to a small-scale, biased real-tumor validation set.

5.2 Overfitting is Alleviated by Large-Scale, Synthetic-Tumor Validation

The overfitting can be alleviated by a diverse, large-scale synthetic-tumor validation set. We conducted a similar experiment to § 5.1. This experiment involved evaluating all the model checkpoints in synthetic-tumor validation set (cohort 5), in-domain test set (cohort 3) and out-domain test set (cohort 7).

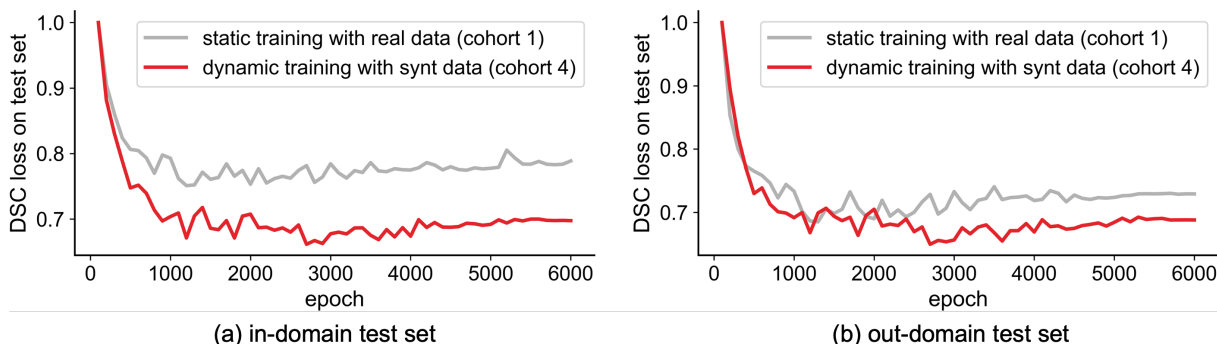
The evaluation trajectory can be observed in Figure 3, with the synthetic-tumor validation set represented by the red line. It is clear that the best checkpoint selected using the synthetic-tumor validation set performs much better than the best checkpoint chosen using the real-tumor validation set when tested with unseen data. Notably, this improvement is especially remarkable when dealing with out-domain data (cohort 7), as the selected model checkpoint is identical to the one chosen by the out-domain test set. These findings emphasize the effectiveness of synthetic-tumor validation set, which serves as a superior alternative to mitigate overfitting issues.

5.3 Overfitting Can Be Addressed by Continual Learning on Synthetic Data

We have shown the effectiveness of large-scale synthetic-tumor validation set. Now, we will shift our attention to synthetic data in handling the overfitting problem from a training perspective. For this purpose, we introduce a continual learning framework on synthetic data, detailed in § 3.1.

The training trajectory of static training on real data and dynamic training on synthetic data is shown in Figure 4, and the liver tumor segmentation results are presented in Table 2. Specifically, the AI model trained on static real data demonstrates a DSC score of 26.7% for the in-domain test set (cohort 3) and 31.1% for the out-domain test set (cohort 7). In comparison, the AI model developed using our continual learning framework with synthetic data achieves notably higher DSC scores, reaching 34.5% on cohort 3 and 35.4% on cohort 7, respectively. These results indicate a notable improvement in the synthetic data. Based on these findings, we can confidently assert that

Figure 4: **The overfitting can be addressed by continual learning on synthetic data.** We set up the continual learning framework for liver tumor segmentation, described in §3.1. Its learning curves are presented in red, referred to as *dynamic training*. In comparison, gray curves are the conventional framework training with a limited number of real data, referred to as *static training*. Both in-domain (a) and out-domain (b) evaluations show that the AI model continuously trained on synthetic data outperforms the one trained on real data.



	evaluated on real data		evaluated on synthetic data	
	train @ real	train @ synt	train @ real	train @ synt
cohort 3	26.7 (22.6-30.9)	33.4 (28.7-38.0)	27.0 (23.7-30.3)	34.5 (30.8-38.2)
cohort 7	31.1 (26.0-36.2)	33.3 (30.6-36.0)	32.0 (28.5-35.5)	35.4 (32.1-38.7)

Table 2: **Synthetic data for both training and validation.** As shown in Figure 4, AI model can be trained on either static real data or dynamic synthetic data. The terms “train @ real” and “train @ synt” denote static training with real data and dynamic training with synthetic data, respectively. We save the model checkpoints at each training epoch and then use a validation set to select the *best* model. These selected model checkpoints are tested on the in-domain LiTS test set (cohort 3) and out-domain FLARE’23 test set (cohort 7). We report the DSC score (%) and 95% confidence interval achieved on the test set. The result reveals that training and validating AI models with our continual learning framework can significantly improve liver tumor segmentation.

incorporating our continual learning framework with synthetic data allows us to effectively address the issue of overfitting, encompassing both the training and validation perspectives.

5.4 Synthetic Data Can Benefit Early Cancer Detection

Early tumor (radius < 5mm) detection plays a critical role in clinical applications, providing valuable information for early cancer diagnosis. Acquiring real data of such a small size is challenging, often posing difficulties or even making it impossible to acquire them. However, our strategy can dynamically generate numerous tiny tumors as required. As a result, the AI model developed within the continual learning framework yields a significant improvement in detecting tiny liver tumors. The improvement can be found in Figure 5. We assessed the sensitivity of the AI model under different settings. The performance of the AI model trained and validated on the static real data is 33.1% for the in-domain test set (cohort 3) and 33.9% for the out-domain test set (cohort 7). Comparatively, the AI model developed using our continual learning framework on synthetic data gives a sensitivity of 55.4% for cohort 3 and 52.3% for cohort 7. These results prove the effectiveness of our framework in early detection of cancer.

5.5 Continual Learning Framework is Enhanced by In-domain Synthetic-Tumor Validation

We have demonstrated the effectiveness of our continual learning framework. Moving forward, let’s consider the framework itself. Synthetic data offers a significant advantage as we can utilize healthy CT volumes from various domains. A notable scenario arises wherein we can directly generate synthetic-tumor validation using healthy cases from the same domain as the test set, providing valuable insights for our continual learning framework. As shown in Figure 6, the in-domain synthetic-tumor validation set showcases its capability to accurately identify the best model, which aligns with the model selected by the test set. This result highlights that the continual learning framework yields more favorable outcomes when we can generate in-domain synthetic-tumor validation.

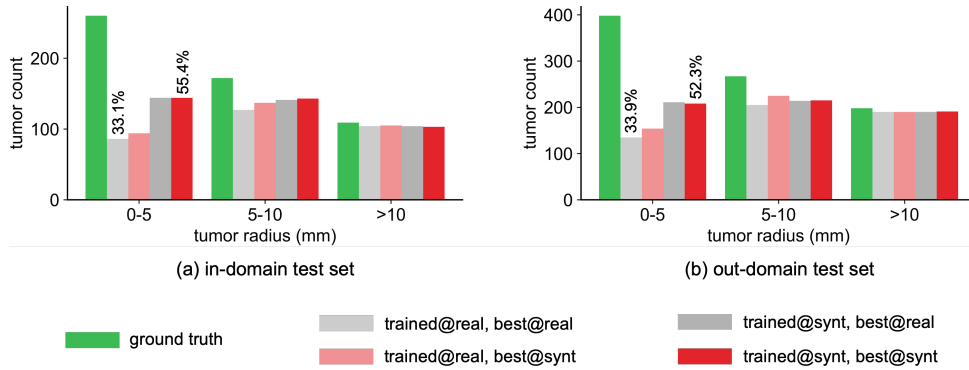


Figure 5: **Synthetic data can benefit early cancer detection.** We evaluate the efficacy of synthetic data in detecting tiny liver tumors (radius < 5mm). Specifically, the AI model developed with our continual learning framework – trained and evaluated with synthetic data – is evaluated on tumor detection. We compare it with AI model developed on static real data. The “trained@real“ and “trained@synt“ hold the same meaning as described in Table 2. The “best@real“ and “best@synt“ denote the selection of best checkpoints based on real- and synthetic- tumor validation sets, respectively. We report the sensitivities (%) achieved on the test set. As shown in both in-domain (a) and out-domain (b) evaluations, our continual learning framework with synthetic data proves to be effective in detecting tiny liver tumors (radius < 5mm), thereby benefiting early cancer detection.

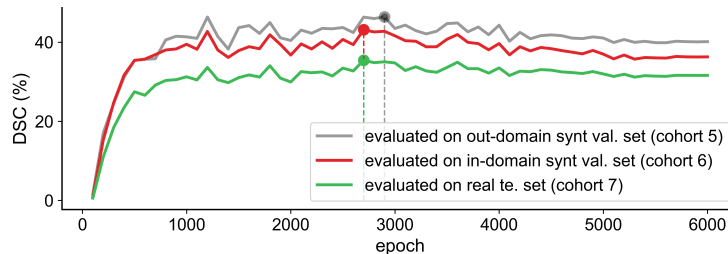


Figure 6: **The continual learning framework is enhanced by in-domain synthetic-tumor validation.** Our framework enables the utilization of healthy cases from various domains. Specifically, an interesting situation arises where we can directly create synthetic-tumor validation using healthy cases from the same domain as the test set. This in-domain synthetic-tumor validation set can benefit our continual learning framework. To illustrate this advantage, we utilize the FLARE’23 dataset, which contains both disease cases and healthy cases. We trained the model using dynamic synthetic data and saved model checkpoints at each training epoch. Subsequently, we evaluated them on three datasets, i.e., out-domain synthetic-tumor validation set from assembly dataset (cohort 5, gray curve), in-domain synthetic-tumor validation set from FLARE’23 dataset (cohort 6, red curve), and FLARE’23 test set served as the gold standard (cohort 7, green curve). As shown, the in-domain synthetic-tumor validation set accurately identifies the best model, which aligns with the model selected by the FLARE’23 test set.

6 Conclusion

Data synthesis strategies continue to pique the interest of researchers and practitioners, propelling ongoing investigations within this field. This paper justifies the potential and stresses the necessity of leveraging synthetic data as validation to select the best model checkpoint along the training trajectory. Moreover, by employing a continual learning framework on synthetic data, we realize a marked improvement in liver tumor segmentation as well as in the early detection of cancerous tumors compared with the static training on real data, where procuring ample annotated examples can be cost-prohibitive. It is particularly valuable in scenarios characterized by limited annotated data. In the future, we plan to improve the generation of synthetic tumors and verify our findings across different organs, such as the pancreas, kidneys, and stomach.

Acknowledgments

This work was supported by the Lustgarten Foundation for Pancreatic Cancer Research and the Patrick J. McGovern Foundation Award. We appreciate the effort of the MONAI Team to provide open-source code for the community. This work has partially utilized the GPUs provided by ASU Research Computing and NVIDIA. We thank Yu-Cheng Chou, Junfei Xiao, Xiaoxi Chen, and Bowen Li for their constructive suggestions at several stages of the project.

References

- [1] Shekoofeh Azizi, Simon Kornblith, Chitwan Saharia, Mohammad Norouzi, and David J Fleet. 2023. Synthetic data from diffusion models improves imagenet classification. *arXiv preprint arXiv:2304.08466*.
- [2] Patrick Bilic, Patrick Ferdinand Christ, Eugene Vorontsov, Grzegorz Chlebus, Hao Chen, Qi Dou, Chi-Wing Fu, Xiao Han, Pheng-Ann Heng, Jürgen Hesser, et al. 2019. The liver tumor segmentation benchmark (lits). *arXiv preprint arXiv:1901.04056*.
- [3] Michael J Black, Priyanka Patel, Joachim Tesch, and Jinlong Yang. 2023. Bedlam: A synthetic dataset of bodies exhibiting detailed lifelike animated motion. In *Proceedings of the IEEE/CVF Conference on Computer Vision and Pattern Recognition*, pages 8726–8737.
- [4] Tom Brown, Benjamin Mann, Nick Ryder, Melanie Subbiah, Jared D Kaplan, Prafulla Dhariwal, Arvind Neelakantan, Pranav Shyam, Girish Sastry, Amanda Askell, et al. 2020. Language models are few-shot learners. *Advances in neural information processing systems*, 33:1877–1901.
- [5] Max F Burg, Florian Wenzel, Dominik Zietlow, Max Horn, Osama Makansi, Francesco Locatello, and Chris Russell. 2023. A data augmentation perspective on diffusion models and retrieval. *arXiv preprint arXiv:2304.10253*.
- [6] Richard J Chen, Ming Y Lu, Tiffany Y Chen, Drew FK Williamson, and Faisal Mahmood. 2021. Synthetic data in machine learning for medicine and healthcare. *Nature Biomedical Engineering*, 5(6):493–497.
- [7] Yuhua Chen, Wen Li, Xiaoran Chen, and Luc Van Gool. 2019. Learning semantic segmentation from synthetic data: A geometrically guided input-output adaptation approach. In *Proceedings of the IEEE/CVF conference on computer vision and pattern recognition*, pages 1841–1850.
- [8] Victoria Chernyak, Kathryn J Fowler, Aya Kamaya, Ania Z Kielar, Khaled M Elsayes, Mustafa R Bashir, Yuko Kono, Richard K Do, Donald G Mitchell, Amit G Singal, An Tang, and Claude B Sirlin. 2018. Liver imaging reporting and data system (LI-RADS) version 2018: Imaging of hepatocellular carcinoma in at-risk patients. *Radiology*, 289(3):816–830.
- [9] Ronan Collobert and Jason Weston. 2008. A unified architecture for natural language processing: Deep neural networks with multitask learning. In *Proceedings of the 25th international conference on Machine learning*, pages 160–167.
- [10] David Crosby, Sangeeta Bhatia, Kevin M Brindle, Lisa M Coussens, Caroline Dive, Mark Emberton, Sadik Esener, Rebecca C Fitzgerald, Sanjiv S Gambhir, Peter Kuhn, et al. 2022. Early detection of cancer. *Science*, 375(6586):eaay9040.
- [11] Cong Gao, Benjamin D Killeen, Yicheng Hu, Robert B Grupp, Russell H Taylor, Mehran Armand, and Mathias Unberath. 2023. Synthetic data accelerates the development of generalizable learning-based algorithms for x-ray image analysis. *Nature Machine Intelligence*, 5(3):294–308.
- [12] James Gareth, Witten Daniela, Hastie Trevor, and Tibshirani Robert. 2013. *An introduction to statistical learning: with applications in R*. Springer.
- [13] Chris A Glasbey and Kantilal Vardichand Mardia. 1998. A review of image-warping methods. *Journal of applied statistics*, 25(2):155–171.
- [14] Rafael C Gonzalez. 2009. *Digital image processing*. Pearson education india.
- [15] Izabela Horvath, Johannes Paetzold, Oliver Schoppe, Rami Al-Maskari, Ivan Ezhov, Suprosanna Shit, Hongwei Li, Ali Ertürk, and Bjoern Menze. 2022. Metgan: Generative tumour inpainting and modality synthesis in light sheet microscopy. In *Proceedings of the IEEE/CVF Winter Conference on Applications of Computer Vision*, pages 227–237.
- [16] Qixin Hu, Yixiong Chen, Junfei Xiao, Shuwen Sun, Jieneng Chen, Alan L Yuille, and Zongwei Zhou. 2023. Label-free liver tumor segmentation. In *Proceedings of the IEEE/CVF Conference on Computer Vision and Pattern Recognition*, pages 7422–7432.
- [17] Qixin Hu, Junfei Xiao, Yixiong Chen, Shuwen Sun, Jie-Neng Chen, Alan Yuille, and Zongwei Zhou. 2022. Synthetic tumors make ai segment tumors better. *NeurIPS Workshop on Medical Imaging meets NeurIPS*.
- [18] Wengong Jin, Regina Barzilay, and Tommi Jaakkola. 2018. Junction tree variational autoencoder for molecular graph generation. In *International conference on machine learning*, pages 2323–2332. PMLR.
- [19] Justin Johnson, Bharath Hariharan, Laurens Van Der Maaten, Li Fei-Fei, C Lawrence Zitnick, and Ross Girshick. 2017. Clevr: A diagnostic dataset for compositional language and elementary visual reasoning. In *Proceedings of the IEEE conference on computer vision and pattern recognition*, pages 2901–2910.

- [20] James Jordon, Lukasz Szpruch, Florimond Houssiau, Mirko Bottarelli, Giovanni Cherubin, Carsten Maple, Samuel N Cohen, and Adrian Weller. 2022. Synthetic data—what, why and how? *arXiv preprint arXiv:2205.03257*.
- [21] James Jordon, Jinsung Yoon, and Mihaela Van Der Schaar. 2018. Pate-gan: Generating synthetic data with differential privacy guarantees. In *International conference on learning representations*.
- [22] Mintong Kang, Bowen Li, Zengle Zhu, Yongyi Lu, Elliot K Fishman, Alan Yuille, and Zongwei Zhou. 2023. Label-assemble: Leveraging multiple datasets with partial labels. In *2023 IEEE 20th International Symposium on Biomedical Imaging (ISBI)*, pages 1–5. IEEE.
- [23] Max Kuhn, Kjell Johnson, et al. 2013. *Applied predictive modeling*, volume 26. Springer.
- [24] B Landman, Z Xu, J Igelsias, M Styner, T Langerak, and A Klein. 2015. 2015 miccai multi-atlas labeling beyond the cranial vault workshop and challenge. doi:10.7303/syn3193805.
- [25] KHY Lee, ME O’Malley, MA Haider, and A Hanbidge. 2004. Triple-phase mdct of hepatocellular carcinoma. *American Journal of Roentgenology*, 182(3):643–649.
- [26] Bowen Li, Yu-Cheng Chou, Shuwen Sun, Hualin Qiao, Alan Yuille, and Zongwei Zhou. 2023. Early detection and localization of pancreatic cancer by label-free tumor synthesis. *MICCAI Workshop on Big Task Small Data, 1001-AI*.
- [27] Cong Liu, Casey N Ta, Jim M Havrilla, Jordan G Nestor, Matthew E Spotnitz, Andrew S Geneslaw, Yu Hu, Wendy K Chung, Kai Wang, and Chunhua Weng. 2022. Oard: Open annotations for rare diseases and their phenotypes based on real-world data. *The American Journal of Human Genetics*, 109(9):1591–1604.
- [28] Jie Liu, Yixiao Zhang, Jie-Neng Chen, Junfei Xiao, Yongyi Lu, Bennett A Landman, Yixuan Yuan, Alan Yuille, Yucheng Tang, and Zongwei Zhou. 2023a. Clip-driven universal model for organ segmentation and tumor detection. In *Proceedings of the IEEE/CVF International Conference on Computer Vision*, pages 21152–21164.
- [29] Qihao Liu, Adam Kortylewski, and Alan L Yuille. 2023b. Poseexaminer: Automated testing of out-of-distribution robustness in human pose and shape estimation. In *Proceedings of the IEEE/CVF Conference on Computer Vision and Pattern Recognition*, pages 672–681.
- [30] Lorenzo Luzi, Ali Siahkoohi, Paul M Mayer, Josue Casco-Rodriguez, and Richard Baraniuk. 2022. Boomerang: Local sampling on image manifolds using diffusion models. *arXiv preprint arXiv:2210.12100*.
- [31] Fei Lyu, Mang Ye, Jonathan Frederik Carlsen, Kenny Erleben, Sune Darkner, and Pong C Yuen. 2022. Pseudo-label guided image synthesis for semi-supervised covid-19 pneumonia infection segmentation. *IEEE Transactions on Medical Imaging*.
- [32] Jun Ma, Yao Zhang, Song Gu, Xingle An, Zhihe Wang, Cheng Ge, Congcong Wang, Fan Zhang, Yu Wang, Yinan Xu, et al. 2022. Fast and low-gpu-memory abdomen ct organ segmentation: the flare challenge. *Medical Image Analysis*, 82:102616.
- [33] Jiteng Mu, Weichao Qiu, Gregory D Hager, and Alan L Yuille. 2020. Learning from synthetic animals. In *Proceedings of the IEEE/CVF Conference on Computer Vision and Pattern Recognition*, pages 12386–12395.
- [34] Aaron van den Oord, Sander Dieleman, Heiga Zen, Karen Simonyan, Oriol Vinyals, Alex Graves, Nal Kalchbrenner, Andrew Senior, and Koray Kavukcuoglu. 2016. Wavenet: A generative model for raw audio. *arXiv preprint arXiv:1609.03499*.
- [35] Senthil Purushwalkam, Pedro Morgado, and Abhinav Gupta. 2022. The challenges of continuous self-supervised learning. In *European Conference on Computer Vision*, pages 702–721. Springer.
- [36] Chongyu Qu, Tiezheng Zhang, Hualin Qiao, Jie Liu, Yucheng Tang, Alan Yuille, and Zongwei Zhou. 2023. Abdomenatlas-8k: Annotating 8,000 abdominal ct volumes for multi-organ segmentation in three weeks. *Conference on Neural Information Processing Systems*.
- [37] Aditya Ramesh, Mikhail Pavlov, Gabriel Goh, Scott Gray, Chelsea Voss, Alec Radford, Mark Chen, and Ilya Sutskever. 2021. Zero-shot text-to-image generation. *arXiv preprint arXiv:2102.12092*.
- [38] Brian D Ripley. 2007. *Pattern recognition and neural networks*. Cambridge university press.
- [39] Olaf Ronneberger, Philipp Fischer, and Thomas Brox. 2015. U-net: Convolutional networks for biomedical image segmentation. In *International Conference on Medical Image Computing and Computer-Assisted Intervention*, pages 234–241. Springer.

- [40] Holger Roth, Amal Farag, Evrim B. Turkbey, Le Lu, Jiamin Liu, and Ronald M. Summers. 2016. [Data from pancreas-ct](https://doi.org/10.7937/K9/TCIA.2016.tNB1kqBU). The Cancer Imaging Archive. <https://doi.org/10.7937/K9/TCIA.2016.tNB1kqBU>.
- [41] Stuart J Russell. 2010. *Artificial intelligence a modern approach*. Pearson Education, Inc.
- [42] Younghak Shin, Hemin Ali Qadir, and Ilangko Balasingham. 2018. Abnormal colon polyp image synthesis using conditional adversarial networks for improved detection performance. *IEEE Access*, 6:56007–56017.
- [43] Yucheng Tang, Dong Yang, Wenqi Li, Holger R Roth, Bennett Landman, Daguang Xu, Vishwesh Nath, and Ali Hatamizadeh. 2022. Self-supervised pre-training of swin transformers for 3d medical image analysis. In *Proceedings of the IEEE/CVF Conference on Computer Vision and Pattern Recognition*, pages 20730–20740.
- [44] Vanya V Valindria, Nick Pawlowski, Martin Rajchl, Ioannis Lavdas, Eric O Aboagye, Andrea G Rockall, Daniel Rueckert, and Ben Glocker. 2018. Multi-modal learning from unpaired images: Application to multi-organ segmentation in ct and mri. In *2018 IEEE winter conference on applications of computer vision (WACV)*, pages 547–556. IEEE.
- [45] Guido M Van de Ven and Andreas S Tolias. 2019. Three scenarios for continual learning. *arXiv preprint arXiv:1904.07734*.
- [46] Guido M Van de Ven, Tinne Tuytelaars, and Andreas S Tolias. 2022. Three types of incremental learning. *Nature Machine Intelligence*, 4(12):1185–1197.
- [47] Hualin Wang, Yuhong Zhou, Jiong Zhang, Jianqin Lei, Dongke Sun, Feng Xu, and Xiayu Xu. 2022. Anomaly segmentation in retinal images with poisson-blending data augmentation. *Medical Image Analysis*, page 102534.
- [48] Magnus Wiese, Robert Knobloch, Ralf Korn, and Peter Kretschmer. 2020. Quant gans: deep generation of financial time series. *Quantitative Finance*, 20(9):1419–1440.
- [49] Julian Wyatt, Adam Leach, Sebastian M Schmon, and Chris G Willcocks. 2022. Anoddpm: Anomaly detection with denoising diffusion probabilistic models using simplex noise. In *Proceedings of the IEEE/CVF Conference on Computer Vision and Pattern Recognition*, pages 650–656.
- [50] Xiaodan Xing, Giorgos Papanastasiou, Simon Walsh, and Guang Yang. 2023. Less is more: Unsupervised mask-guided annotated ct image synthesis with minimum manual segmentations. *IEEE Transactions on Medical Imaging*.
- [51] Qingsong Yao, Li Xiao, Peihang Liu, and S Kevin Zhou. 2021. Label-free segmentation of covid-19 lesions in lung ct. *IEEE Transactions on Medical Imaging*.
- [52] Jinsung Yoon, Daniel Jarrett, and Mihaela Van der Schaar. 2019. Time-series generative adversarial networks. *Advances in neural information processing systems*, 32.
- [53] Menghan Yu, Sourabh Kulhare, Courosh Mehanian, Charles B Delahunt, Daniel E Shea, Zohreh Laverriere, Ishan Shah, and Matthew P Horning. 2023. How good are synthetic medical images? an empirical study with lung ultrasound. In *International Workshop on Simulation and Synthesis in Medical Imaging*, pages 75–85. Springer.
- [54] Chenyu Zheng, Guoqiang Wu, and Chongxuan Li. 2023. Toward understanding generative data augmentation. *arXiv preprint arXiv:2305.17476*.
- [55] Zongwei Zhou. 2021. *Towards Annotation-Efficient Deep Learning for Computer-Aided Diagnosis*. Ph.D. thesis, Arizona State University.
- [56] Zongwei Zhou, Michael B Gotway, and Jianming Liang. 2022. Interpreting medical images. In *Intelligent Systems in Medicine and Health*, pages 343–371. Springer.
- [57] Zengle Zhu, Mintong Kang, Alan Yuille, and Zongwei Zhou. 2022. Assembling and exploiting large-scale existing labels of common thorax diseases for improved covid-19 classification using chest radiographs. In *Radiological Society of North America (RSNA)*.

A Distribution of Real Tumors

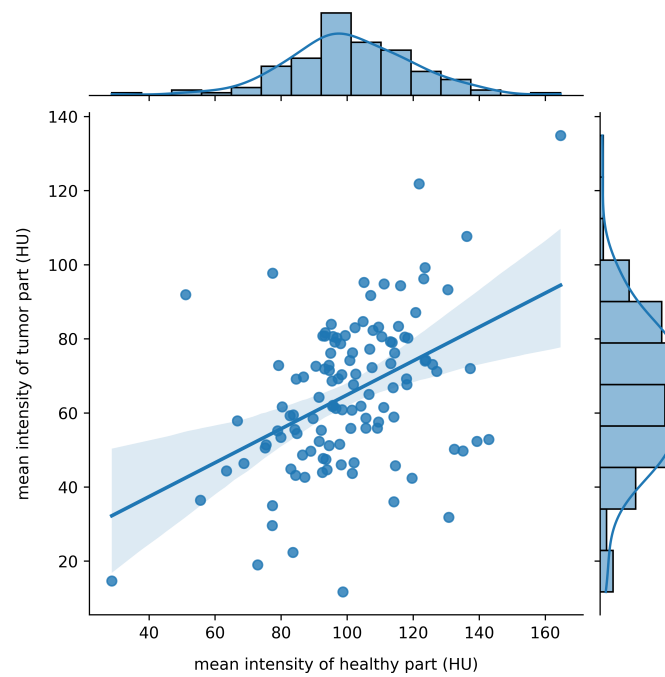


Figure 7: **Intensity distribution of liver tumors and their healthy counterparts.** Our tumor generator, which is based on modeling and medical knowledge, incorporates the distributional characteristics of real tumors. We present the intensity distributions of real tumors obtained from the LiTS dataset.

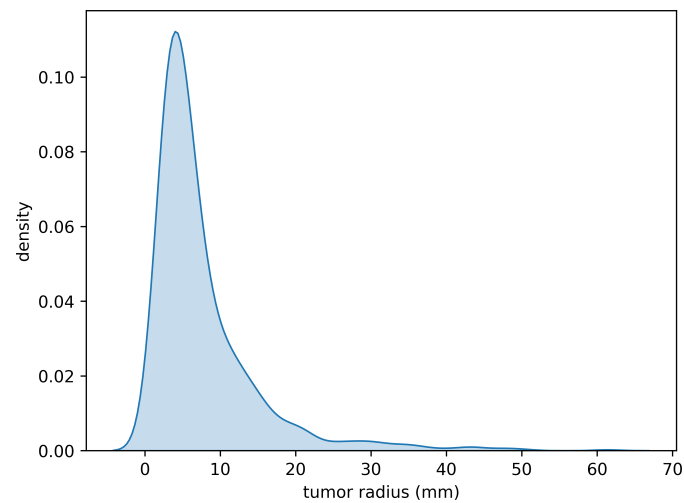


Figure 8: **Size distribution of liver tumors.** We have calculated the size distribution of liver tumors from the LiTS dataset. This tumor size distribution will serve as a guide for determining the sizes of the synthetic tumors we generate.

B Shape Examples

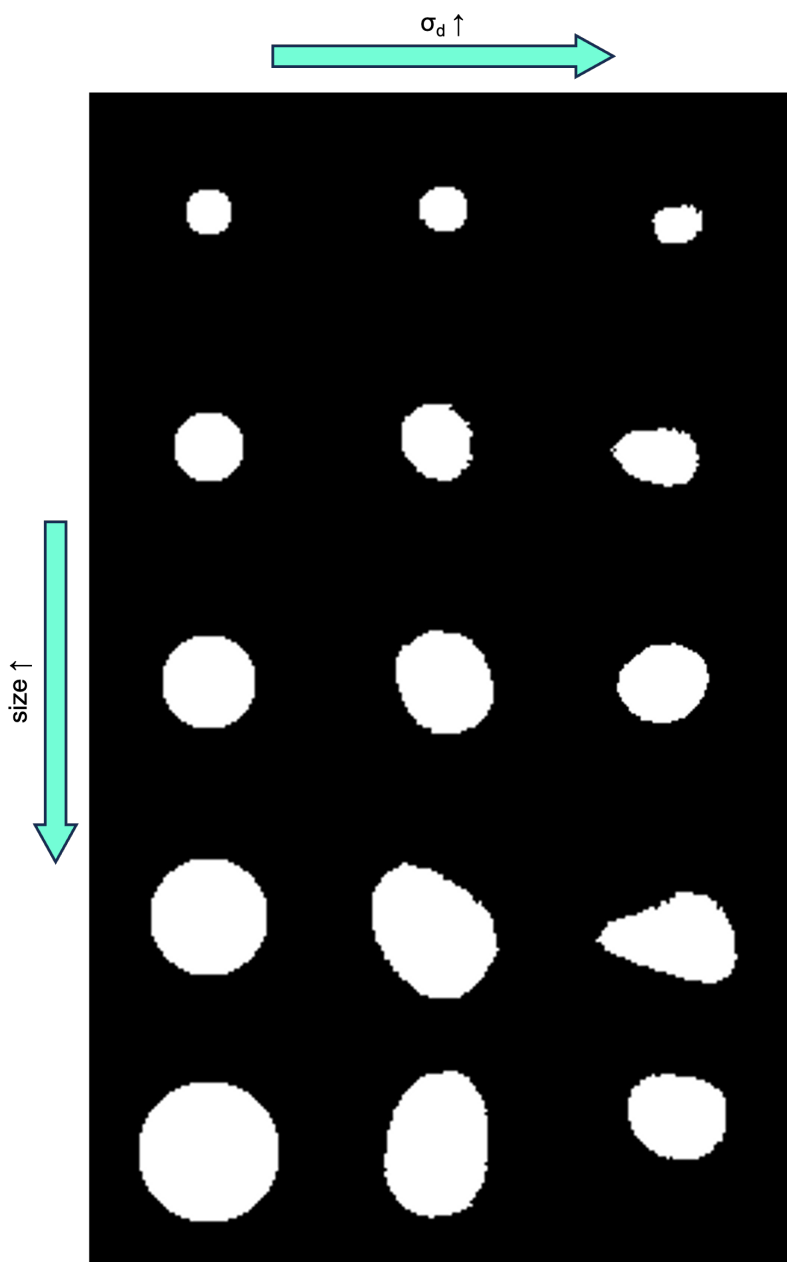


Figure 9: **Examples of the generated shape.** The tumor generator pipeline enables us to control the size and deformation of the generated tumors. Here, we present some examples of generated shapes under different conditions.

C Texture Examples

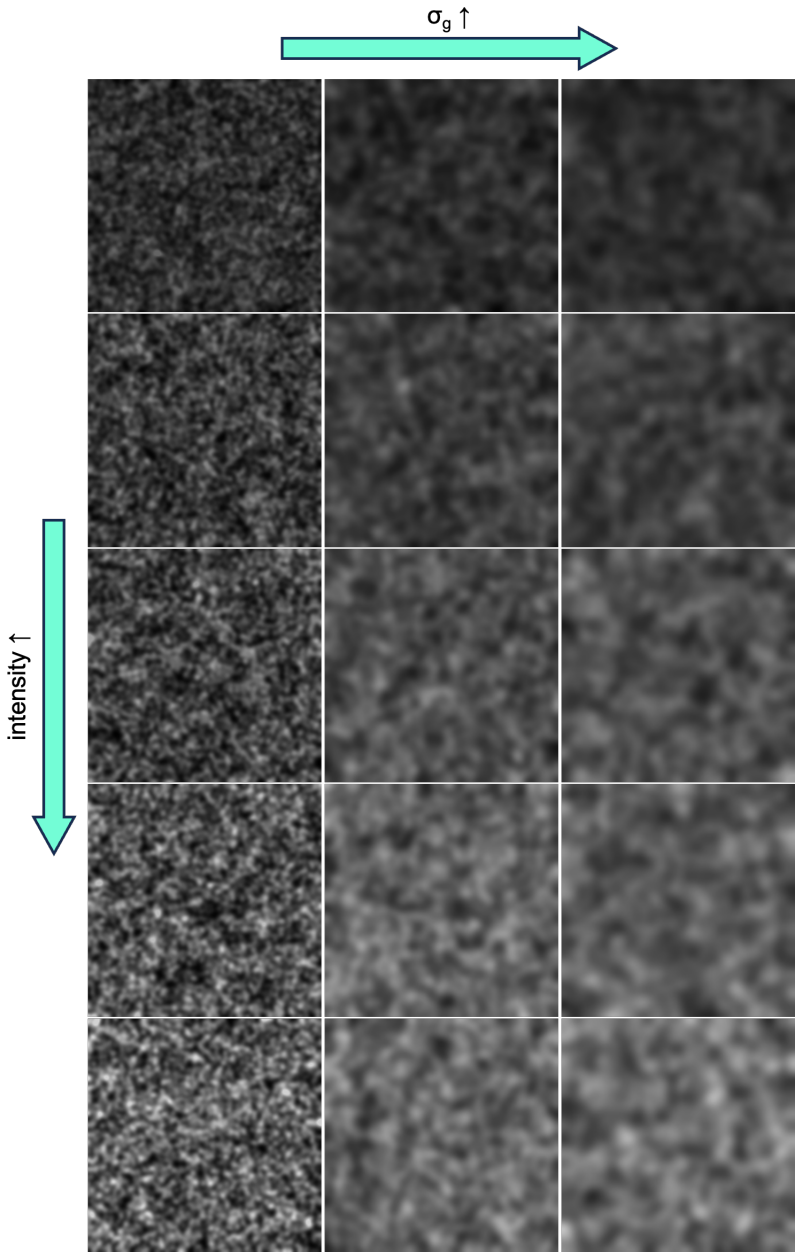


Figure 10: **Examples of the generated texture.** Our data synthesis strategy also enables us to generate different textures, as illustrated here for visualization.

D Synthetic tumor examples

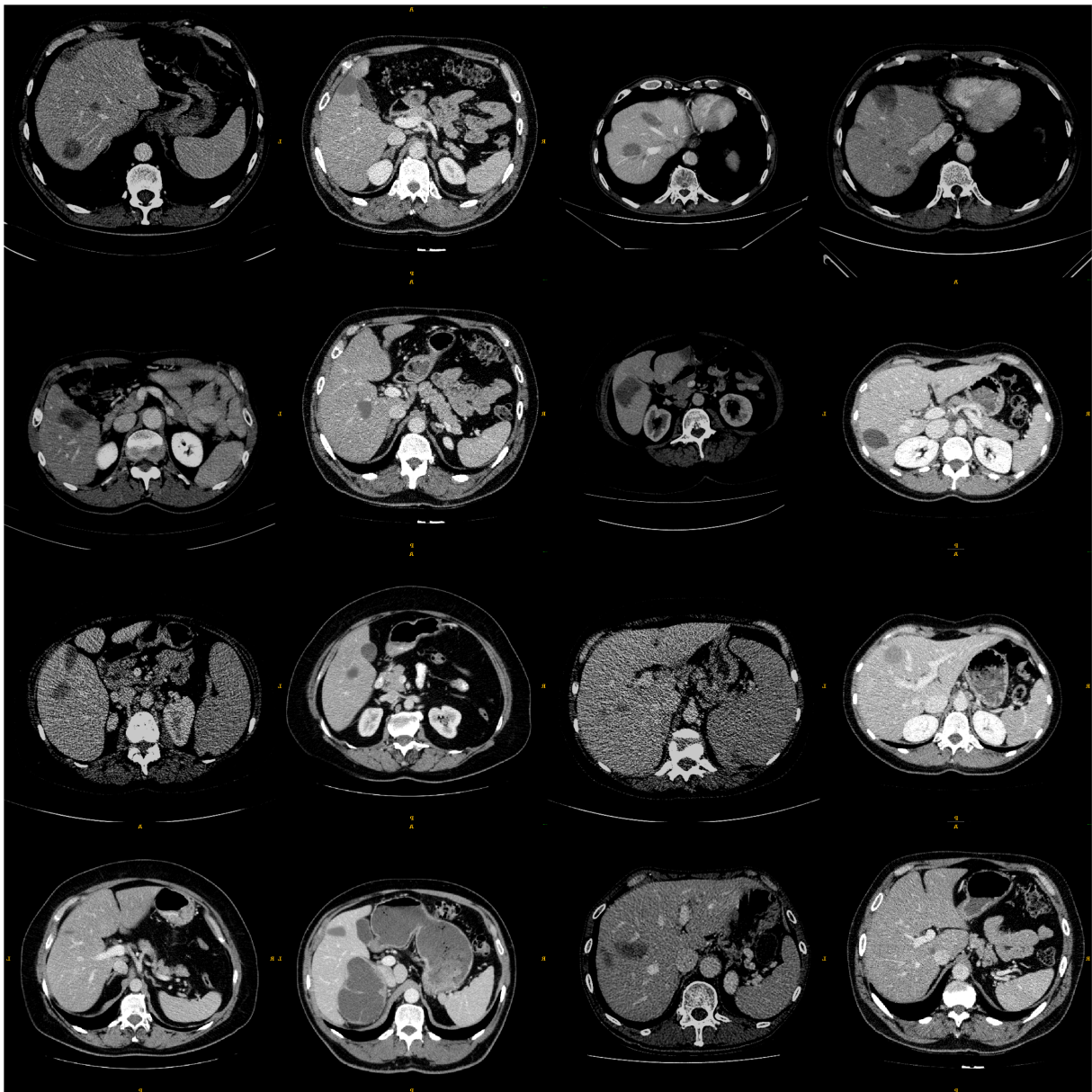


Figure 11: **Visualization of synthetic data.** By combining all the pipelines together, we can obtain a wide range of diverse synthetic data for validation and training.